Electrochimica Acta 525 (2025) 146182

Contents lists available at ScienceDirect

Electrochimica Acta

journal homepage: www.journals.elsevier.com/electrochimica-acta

Experimental assessment of different reactor configuration approaches for direct CO_2 electroreduction to formic acid

Jose Antonio Abarca *, Mario Coz-Cruz, Manuel Alvarez-Guerra, Guillermo Díaz-Sainz *, Angel Irabien

Departamento de Ingenierías Química y Biomolecular, Universidad de Cantabria, Avenida de los Castros s/n, 39005 Santander, Spain

ARTICLE INFO

Keywords:
CO_2 electroreduction
Electrolyzer configuration
Formic acid
Bipolar membrane
Three-compartment reactor

ABSTRACT

Electrochemical CO_2 conversion is a promising technology for reducing industrial CO_2 emissions. The conversion of CO_2 to formic acid (HCOOH) typically requires an intermediate acidolysis step when conventional CO_2 electrolyzers produce formate. Developing reactors capable of directly producing HCOOH production could significantly enhance the scalability of CO_2 electroreduction. This study evaluates and compares two reactor configurations: (i) a three-compartment reactor and (ii) a two-compartment electrolyzer with a bipolar membrane. In the three-compartment reactor, the effects of current density, CO_2 flow rate, and water content in the CO_2 gas feed are analyzed, thus they are scarcely explored yet. Under optimal conditions, a current density of 200 mA cm^{-2}, a CO_2 flow rate of 20 mL min^{-1}, 0.5 g h^{-1} of water content, HCOOH concentration of 125 g L^{-1} with 57 % Faradaic Efficiency, and an energy consumption of 368 kWh $kmol^{-1}$ are achieved. In the two-compartment electrolyzer, various catholyte solutions (0.1 M KCl and 0.5 M $KHCO_3$) are tested to assess the impact of current density and flow rate. The best results are obtained with 0.1 M KCl at a current density of 90 mA cm^{-2} and a flow rate of 0.15 mL min^{-1} cm^{-2}, producing 5.28 g L^{-1} of HCOOH with a Faradaic Efficiency of 62 %. However, energy consumption is higher at 572 kWh $kmol^{-1}$ due to the overpotential required for water dissociation in the bipolar membrane. These findings demonstrate the potential of both reactor designs for advancing industrial CO_2 electroreduction to HCOOH, with unique trade-offs between efficiency and energy consumption in each configuration.

1. Introduction

Climate change is one of the most significant challenges faced by society in the 21st century. It refers to the long-term alteration of climate patterns and atmospheric temperatures. The extensive use of fossil fuels for energy and other anthropogenic activities such as agriculture, transportation, and industry, has led to a substantial increase in carbon dioxide (CO_2) emissions. Recently, atmospheric CO_2 concentration surpassed the 425-ppm threshold [1], representing a 150 % increase compared to preindustrial levels.

To address this issue, numerous approaches have been explored to mitigate CO_2 emissions. These include improving energy efficiency, transitioning to renewable energy sources, and implementing carbon capture and storage (CCS) or carbon capture and utilization (CCU) technologies [2]. Among these, carbon valorization, which converts CO_2 emissions into valuable carbon products, is particularly promising. This approach can be realized through various processes, including thermochemical or mineralization processes [3], as well as photoelectrocatalytic [4], and electrochemical pathways [5].

Electrochemical CO_2 reduction is widely regarded as a promising strategy from both environmental and economic perspectives. This approach enables the storage of surplus renewable energy in chemical bonds while generating valuable products. The specific products obtained from CO_2 reduction depend on factors such as reaction medium, applied voltage, and catalytic material [5]. The process involves applying a potential difference between two electrodes, enabling the transformation of CO_2 into reduced molecules with significant industrial interest. The reduction reaction occurs at the cathode (working electrode), while an oxidation reaction at the anode (counter-electrode) provides the electrons needed for the cathodic half-reactions, ensuring process functionality [6].

To prevent reduced products from diffusing to the anode, where they

* Corresponding authors.
E-mail addresses: joseantonio.abarca@unican.es (J.A. Abarca), guillermo.diazsainz@unican.es (G. Díaz-Sainz).

https://doi.org/10.1016/j.electacta.2025.146182
Received 17 December 2024; Received in revised form 1 April 2025; Accepted 1 April 2025
Available online 6 April 2025

might be reoxidized, an ion exchange membrane is typically placed between the electrodes. This membrane separates the reduction and oxidation reactions while allowing the transfer of specific charged species.

Formic acid (HCOOH) and formate ($HCOO^-$) are two key CO_2 reduction products with significant industrial relevance. They serve as precursors for high-value products and raw materials for fuel cell applications. Common industrial uses include silage preservation, animal feed additives, textile finishing, antifreeze agents, and intermediates in the chemical and pharmaceutical industries [7,8]. Formic acid is particularly attractive due to its unique role in many applications. Global demand for HCOOH is expected to rise significantly, from 750,000 tons in 2021 to 1300,000 tons by 2035, driven by advancements in emerging technologies [9].

The configuration of the electrochemical reactor plays a critical role in the efficient electrochemical reduction of CO_2 to HCOOH and $HCOO^-$. Reactors can operate in batch [10,11], semi-batch [12] or continuous operation mode [13]. Among these, filter press-type or flow cell reactors are the most studied, with two-compartment and three-compartment designs being the most common [14]. While two-compartment reactors have been extensively researched [15–19], three-compartment reactors represent a novel and evolving approach [20–23]. On one hand, two-compartment reactors with an MEA configuration achieve higher product concentrations (in this case, formate) and lower cell potential due to the shorter distance between electrodes, which reduces ohmic resistance [24]. However, the stability of these systems presents a significant challenge, as electrode deactivation occurs within a few hours of operation due to phenomena such as salt deposition or electrode flooding [25,26]. On the other hand, three-compartment reactors can directly produce formic acid, eliminating the need for an intermediate acidolysis step [27], and have shown excellent stability, as cation migration and salt precipitation are prevented by the use of an AEM adjacent to the cathode [28]. However, their main drawbacks include operational and construction complexity due to their internal structure, in which the ion-exchange resin plays a crucial role, making scaling up more challenging.

In two-compartment reactors (Fig. 1), components such as electrodes, current collectors, separators, flow distributors, and housings create distinct cathodic and anodic compartments separated by an ion exchange membrane. This membrane may be cationic (CEM), anionic (AEM), or bipolar (BPM).

CEMs, composed of polymeric materials containing sulfonic, phosphoric, or sulfonamide groups, are the most commonly reported membranes in CO_2 electroreduction ($ERCO_2$) studies [14]. Nafion membranes, in particular, are valued for their selective cation transport capabilities [30–32]. In $ERCO_2$, CEMs concentrate products in the cathode's output stream by limiting $HCOO^-$ anion migration to the anode, thereby minimizing product reoxidation [33]. However, at high product concentrations, some diffusion to the anodic compartment can occur, reducing selectivity [34].

AEMs, which permit anion passage due to their positively charged polymer structure, are another option. Commonly used AEMs include those from manufacturers like Fumatech [35,36], Selemion [37,38], and Sustainion [39,40]. While AEMs enable high current densities due to alkaline electrolyte conductivity [38,41], they also risk $HCOO^-$ diffusion, potentially causing re-oxidation at the anode [42].

In recent years, only a few dozen articles have reported the direct production of HCOOH through the electroreduction of CO_2. Among these, a significant number focus on developing catalysts using density functional theory and validating their effectiveness in batch-type H cells [43,18,44,39,45–47]. However, very few studies address the continuous conversion of CO_2 to $HCOO^-$ in flow cells [48,49]. In this context, two main approaches have been explored: (i) using acidic electrolytes to achieve an acidic product stream [50,51], and (ii) employing three-compartment reactors, where formic acid is collected in a central compartment based on a solid electrolyte [13,28,23]. This work investigates and compares both approaches with previously utilized reactor configurations, by utilizing a flow cell with a BPM and a three-compartment reactor.

On the one hand, BPMs, consisting of cation-selective and anion-selective layers, offer improved process efficiency by facilitating water dissociation into hydroxyl ions, which migrate to the anode and cathode [52]. BMPs allow for direct HCOOH production at the reactor outlet [53], although they require higher energy inputs due to the water dissociation overpotentials.

On the other hand, three-compartment reactors represent one of the most innovative configurations in $ERCO_2$. These reactors include a central compartment separated from the cathodic and anodic compartments by an anion membrane and a cation membrane, respectively (Fig. 2). This design enables the direct production of HCOOH in the central compartment. Commonly used membranes include Nafion for the cationic layer and Sustainion for the anionic layer [13]. The inclusion of solid electrolyte materials or ion-exchange resins in the central compartment enhances ionic conductivity. Since deionized water is typically used to maximize product purity, its low conductivity necessitates the addition of a conductive material to maintain adequate ionic transport. Ion exchange resins ensure stable conductivity within the central compartment and help keep cell voltages low [54].

The use of both membranes minimizes carbonate and bicarbonate precipitation on the cathode, ensuring system stability [55]. Although this configuration has demonstrated continuous operation for over 1000 h at the laboratory scale, scalability remains a challenge [28].

Despite significant advances in $ERCO_2$ to formate, particularly in the selection of highly selective catalyst [7,56,57], electrode configuration [58,59,30], and optimization of operating variables such as electrolyte composition [57,60,61], the direct production of HCOOH on a larger

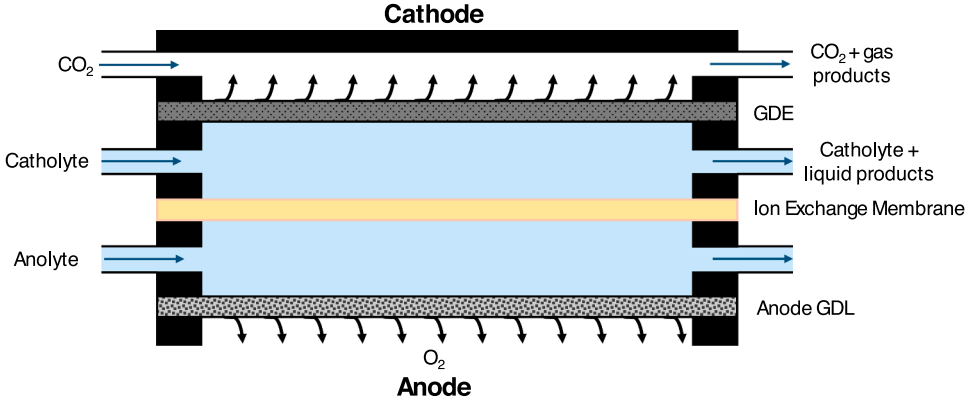

Fig. 1. Scheme of a two-compartment filter-press reactor. Adapted with permission from [29].

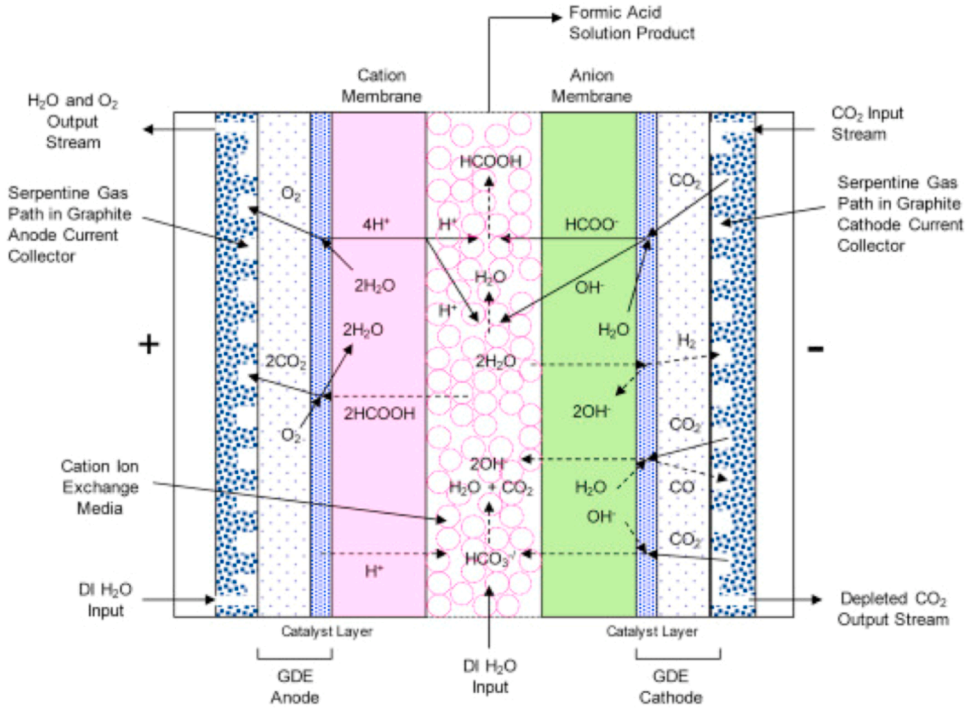

Fig. 2. Three-compartment configuration scheme, illustrating reactions and ion transfer. Adapted with permission from [28].

scale remains limited. Most studies focus on the production of $HCOO^-$ in its anionic form, which requires an intermediate acidolysis step to convert it into HCOOH. This additional step increases both process complexity and costs, creating a significant barrier to industrial implementation.

Although some studies, such as those mentioned earlier, have proposed approaches for directly obtaining HCOOH and achieved noteworthy progress, there remains a critical gap. To the best of the authors' knowledge, no studies have specifically evaluated various reactor configurations while simultaneously examining the influence of key operational variables.

In this regard, this work explores and compares two alternatives: (i) a three-compartment reactor design, which requires further optimization of variables such as water flow rate in the CO_2 gas feed, current density, and CO_2 flow rate; and (ii) the integration of a BPM in a filter-press reactor to acidify the cathodic product stream, enabling direct HCOOH production. Advancing these configurations could represent a significant step toward the industrial scalability of ERCO₂ for HCOOH production, paving the way for efficient CO_2 recycling in industrial settings.

2. Methodology

2.1. Preparation of electrodes for CO_2 electroreduction

The cathode is a GDE consisting of a carbon support and a catalyst layer (CL) combined with a carbon substrate (MPL) (Fig. 3.a) The carbon support is a 50 % Teflon-coated Toray carbon paper (AvCarb MGL 190 – 50wt % PTFE-treated, Fuelcell). The catalytic ink contains 150 mg each of Vulcan XC-72 R and bismuth oxide nanoparticles (Bi_2O_3, particle size 90–210 nm, Sigma-Aldrich), 375 mg of PTFE (polytetrafluoroethylene preparation, 60 wt % dispersion in H_2O, Sigma-Aldrich), and 1.285 mg of Nafion dispersion (Nafion d-521 dispersion, 5 wt % in water and 1-propanol, with an exchange capacity of $\geq$ 0.92 meq·g^{-1}). This mixture is diluted in 25 g of ethanol (Ethanol, 96 % v/v pure, pharmaceutical grade, PanReac AppliChem) and spray-coated onto the carbon paper,

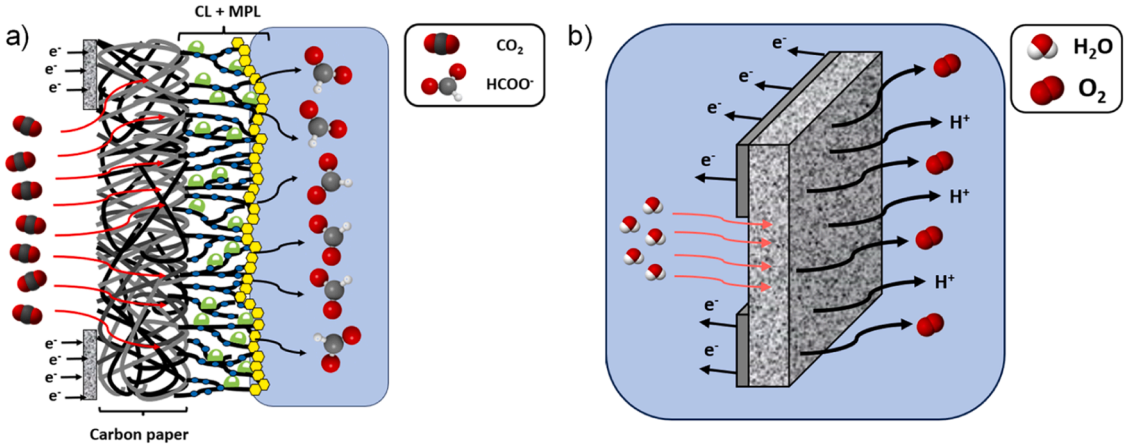

Fig. 3. Schematic of a) GDE used as the cathode, and b) Ni Foam employed as the anode for BPM reactor.

achieving a catalyst loading of 4.0 mg cm^{-2} after thermal treatment at 80 °C for 30 min (Digitronic oven, J. P. Selecta). Before use, the electrode is activated by immersion in a 1 M KOH solution for 1 hour and air-dried [13].

For the three-compartment reactor, the anode is a particulate electrode comprising a carbon-based support and a catalytic ink. The carbon support comprises 5 % Teflon-coated Toray carbon paper (TGP-H-60). The catalytic ink contains iridium oxide (IrO_2) nanoparticles, Nafion (Nafion d-521 Dispersion, 5 % w/w in water and 1-propanol, with an exchange capacity of ≥ 0.92 meq·g^{-1}), and deionized water (MILI-Q), diluted with 1-propanol for deposition. After 30 min of ultrasonic sonication, the ink is spray-coated onto the carbon paper, achieving a catalyst loading of 1.0 mg cm^{-2}, and thermally treated at 80 °C.

In the case of the BPM two compartment reactor, the anode is made of 3D nickel foam (Goodfellow), providing a high surface area to enhance the oxygen evolution reaction (OER) (Fig. 3.b).

2.2. Electrolyzer configurations

This study evaluates reactor configurations for the direct electroreduction of CO_2 to HCOOH, aiming to identify scalable systems with optimal performance. Two reactor configurations are evaluated: (i) three-compartment reactor: this reactor operates with a gaseous CO_2 feed without a liquid catholyte. Reaction products are collected in the central compartment, which is maintained under a continuous deionized water flow; (ii) two-compartment bipolar membrane reactor: this reactor uses a BPM to dissociate water into H^+ and OH^- ions, with a liquid catholyte to facilitate the reaction.

2.3. Three-compartment reactor

A commercial three-compartment reactor (Dioxide Materials) is used, featuring a gas diffusion electrode (GDE) with a 5 cm^2 area serving as the cathode. The reactor has cathodic, anodic, and central compartments separated by ion exchange membranes (Fig. 4). A Sustainion AEM separates the cathodic and central compartments, while a Nafion 324 CEM separates the anodic compartment and central compartments. The central compartment contains ion exchange resins (Amberlite® IR120, hydrogen form, Sigma Aldrich) to facilitate the reaction between $HCOO^-$ anions from the cathode and the protons from the anode.

The cathodic compartment is fed with a humified CO_2 stream, with the water content controlled using a Vapour Delivery Module (VDM, Bronkhost High-Tech B.V). The CO_2 flow rate is varied between 20 and 60 mL min^{-1}, while the water content ranges from 0.2 to 3 g h^{-1}. The experimental variables analyzed, CO_2 flow rate, water content in the CO_2 feed, and current density affecting the $ERCO_2$ performance, are summarized in Table 1. The VDM operates at 60 °C to ensure that the water content in the CO_2 feed does not condense before reaching the reactor inlet.

Pure Milli-Q water is supplied to the anode at a constant flow rate of 3 mL min^{-1}, while the central compartment receives 0.065 mL min^{-1}, following the setup used in previous work with the same reactor configuration [28]. Electrolytes are delivered using two peristaltic pumps: a micropump (HF-LabN3-III, HygiaFlex) for low flow rates and a standard pump (Watson Marlow 320, Watson Marlow Pumps Group) for higher flow rates.

Current densities of 45–200 mA cm^{-2} are applied during galvanostatic operation using a programmable power supply (Programmable Power Supply, MP711009, 30 V, 5A, Multicomp PRO) A schematic representation of the experimental setup is in Figure S1 of the Supporting Information.

2.4. Two-compartment BPM reactor

A commercial filter-press electrochemical reactor (A/S ElectroCell) with a 10 cm^2 geometric area is adapted for a BPM configuration.

The cathode and anode compartments are separated by a BPM (Fumasep FBM-PK), with the cationic side oriented toward the cathode, as shown in Fig. 5. The anolyte is 1 M KOH solution (Potassium hydroxide, 85 % purity, pharmaceutical grade, PanReac AppliChem),

Table 1
Experimental conditions for the three-compartment electrolyzer.

CO_2 flow rate (mL min^{-1})	Water content in CO_2 feed (g h^{-1})	Current density (mA cm^{-2})	Central compartment flow rate (mL min^{-1} cm^{-2})
20	0.2	45, 90, and 200	0.013
	0.5		
	1.5		
	3		
40	0.2		
	0.5		
	1.5		
	3		
60	0.2		
	0.5		
	1.5		
	3		

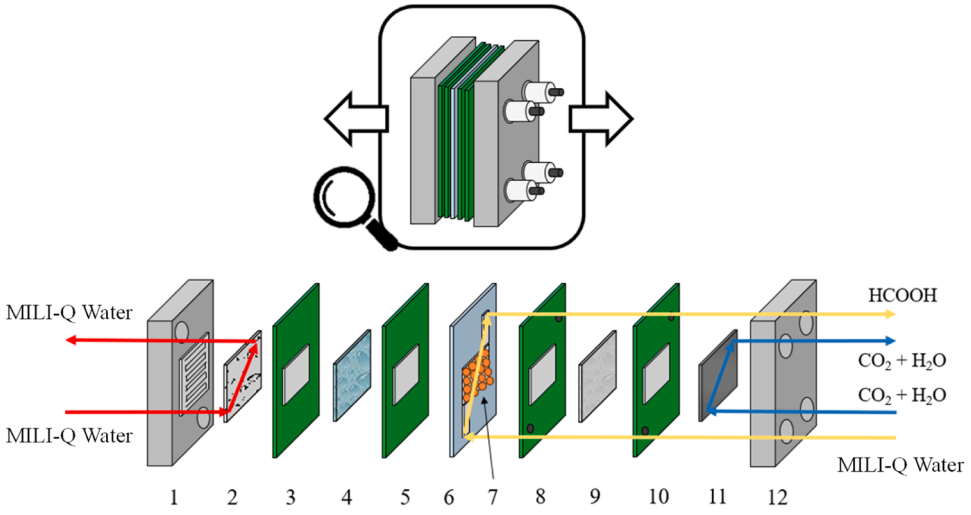

Fig. 4. Schematic of the three-compartment filter-press reactor by Dioxide Materials. 1 and 12) frames; 2) anode; 3, 5, 8, 10) gaskets; 4) Nafion® 324 membrane; 6) central compartment flow distributor; 7) ion exchange resins (Amberlite® IR120); 9) Sustainion membrane; 11) cathode.

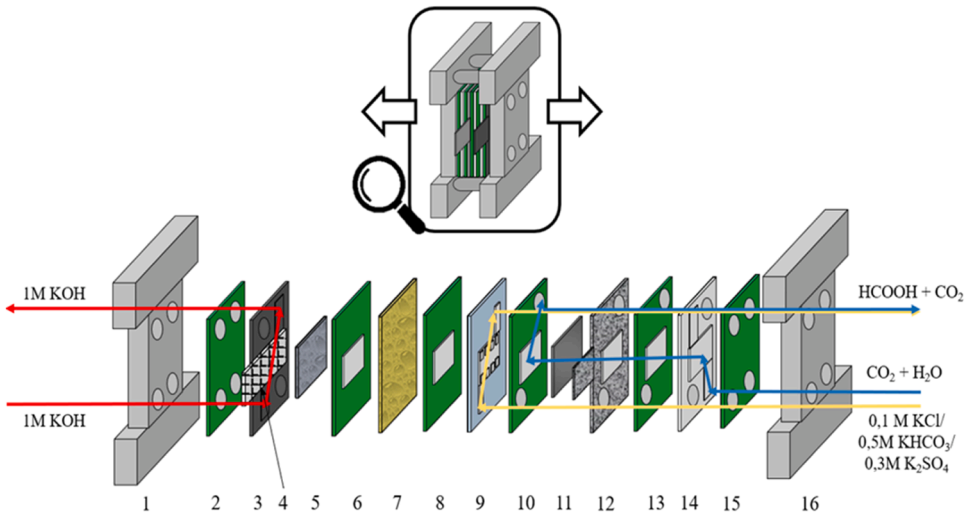

Fig. 5. Schematic representation of the two-compartment filter-press reactor with a bipolar membrane. 1 and 16) frames; 3, 9, 14) flow distributors; 4 and 12) current collectors; 5) anode; 2, 6, 8, 10, 13, 15) gaskets; 7) Fumasep bipolar membrane; 11) cathode.

while the catholyte is either 0.1 M KCl (Potassium chloride, pharmaceutical grade, PanReac AppliChem) or 0.5 M $KHCO_3$ (Potassium bicarbonate, pharmaceutical grade, PanReac AppliChem) to evaluate ion effects and conductivity.

CO_2 is introduced at 200 mL min^{-1}, with a water flow rate of 1.5 g h^{-1}, based on previous works that used this CO_2 feed [62]. A schematic representation of the experimental setup is shown in Figure S2 of the Supplementary Information.

The experimental conditions, including variations in catholyte composition, flow rate, and current density, are summarized in Table 2.

Liquid samples are collected every 20 min during 1-hour experiments. Formate/formic acid concentrations are determined by ion chromatography (Dionex ICS 1100) using an AS9-HC column with a 4.5 mM sodium carbonate eluent at 1 mL min^{-1}. Each experiment is replicated at least twice to ensure that the variability does not exceed 10 % of the Standard Relative Deviation (SRD).

Performance is evaluated regarding Faradaic Efficiency (FE), HCOOH production rate, energy consumption (EC), and single-pass conversion efficiency (SPCE). Detailed calculation methods are provided in the Supporting Information.

3. Results

3.1. Performance analysis of the three-compartment reactor

The performance of the three-compartment reactor is assessed under continuous operation using the experimental set-up and experimental conditions described in the previous section of the methodology. Detailed results of the different experiments are presented in Tables S1-S3 in the Supporting Information.

Table 2
Experimental conditions for the BPM electrolyzer.

Catholyte		Anolyte	CO_2 flowrate (mL min^{-1})	Current density (mA cm^{-2})
Composition	Flow rate (mL min^{-1})			
0.1 M KCl	0.7 1.5 5.7	1 M KOH, 5.7 mL min^{-1}	200 (1.5 g h^{-1} of H_2O)	45, 90 and 200
0.5 M $KHCO_3$	0.7 1.5 5.7			

Preliminary experiments with CO_2 feed rates of 20 and 60 mL min^{-1} show no significant impact on performance, as illustrated in Fig. 6. Therefore, subsequent experiments use a constant CO_2 feed flow rate of 20 mL min^{-1}.

The effects of *j* (45, 90, and 200 mA cm^{-2}) and water vapor flow rates (0.2, 0.5, 1.5, and 3 g h^{-1}), on HCOOH production are investigated (Fig. 7). Results demonstrate that HCOOH concentration and FE are significantly influenced by variations in j and water content. At 45 mA cm^{-2}, the highest concentration and FE (45.4 g L^{-1} and 92 %, respectively) are achieved under a CO_2 feed condition with 0.2 g·h^{-1} water vapor. As expected, increasing the water content reduces HCOOH concentration, reaching 39.3 g l^{-1} at 1.5 g h^{-1}, with a FE of 80 %. Interestingly, at a flow rate of 3 g h^{-1}, a slight increase to 39.73 g L^{-1} is observed, though the FE remains at 80 %. This deviation is attributed to overpressure sensitivity in the central compartment's flow rate (0.013 mL min^{-1} cm^{-2}), impacting production rates.

At *j* of 200 mA cm^{-2}, the highest HCOOH production of 142.5 g L^{-1} and FE of 65 % are obtained with 0.2 g h^{-1} water vapor. As with lower current density, increasing water flow rates lead to decreased HCOOH concentrations (120–125 g l^{-1}) and reduced FE (58–55 %) for water contents above 0.5 g h^{-1} in the CO_2 gas feed.

Energy consumption and HCOOH formation rates as functions of *j* and water vapor flow rates are shown in Fig. 8. At j 45 mA cm^{-2}, energy consumption ranges from 170 to 202 kWh $kmol^{-1}$, with the highest efficiency observed at 0.2 g h^{-1}. At this flow rate, energy consumption is only 170 kWh $kmol^{-1}$, and the production rate is 2.14 mmol m^{-2} s^{-1}. Higher water flow rates increase energy consumption (e.g., 200 kWh $kmol^{-1}$ at 3 g h^{-1}) and reduce production rates (e.g., 1.87 mmol m^{-2} s^{-1}).

At *j* 200 mA cm^{-2}, energy consumption significantly increases (323 −382 kWh $kmol^{-1}$), while production rates vary from 6.72 to 5.67 mmol m^{-2} s^{-1} across water vapor flow rates of 0.2–3 g h^{-1}.

The results reveal that the water content in the CO_2 feed stream critically influences reactor performance. Increasing water content leads to marked declines in HCOOH production efficiency. Specifically, HCOOH concentration decreases from 87.8 g L^{-1} to 59.3 g L^{-1} as water vapor flow rate increases from 0.2 to 3 g h^{-1}, while FE declines from 88 % to 60 %. These effects are attributed to product dilution and the promotion of the hydrogen evolution reaction (HER), which competes with CO_2 reduction under high humidity conditions, reducing HCOOH selectivity [24]. Moreover, it is worth highlighting the SPCE values obtained for this reactor, which demonstrated exceptional performance, achieving CO_2 conversion efficiencies exceeding 27 % in a single pass when operating with an inlet CO_2 feed containing 0.2 g h^{-1} of water at a

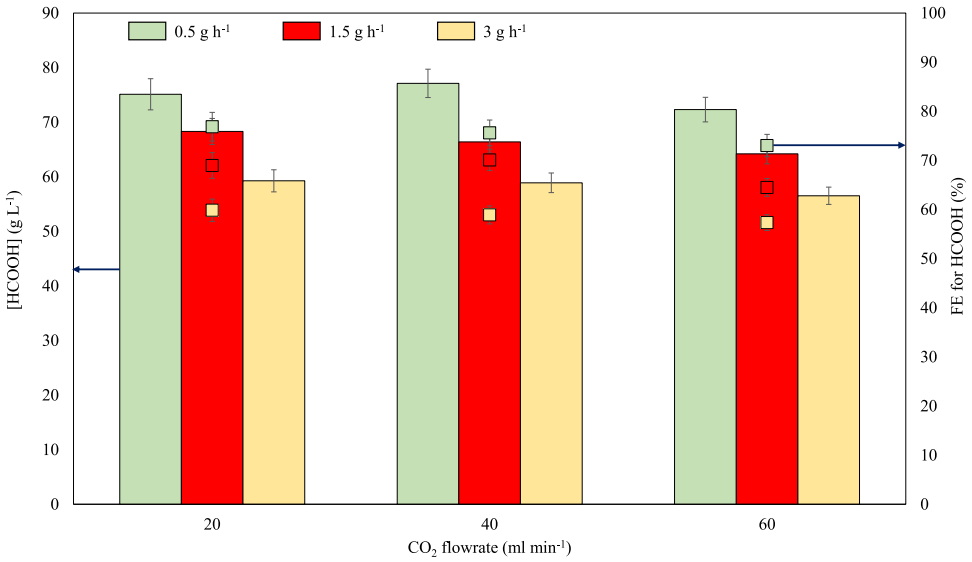

Fig. 6. Three-compartment electrolyzer performance comparison for operation at different CO_2 inlet flow rates and water content in the inlet at 90 mA cm^{-2}.

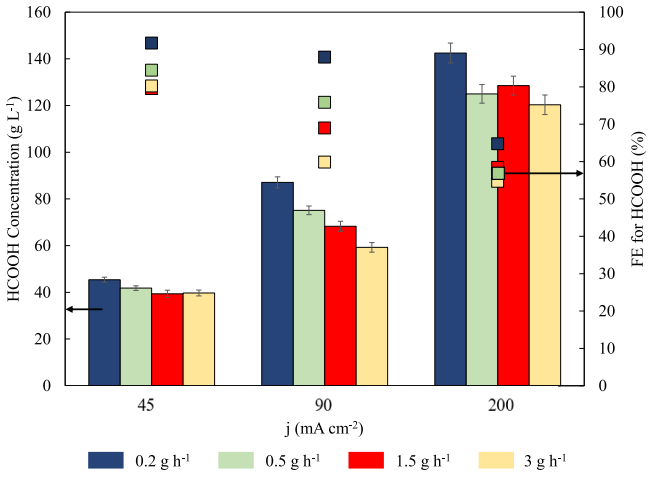

Fig. 7. HCOOH production in terms of concentration and FE in the three-compartment reactor as a function of j and water content in the feed CO_2 stream, with a fixed CO_2 feed flow rate of 20 ml min^{-1}.

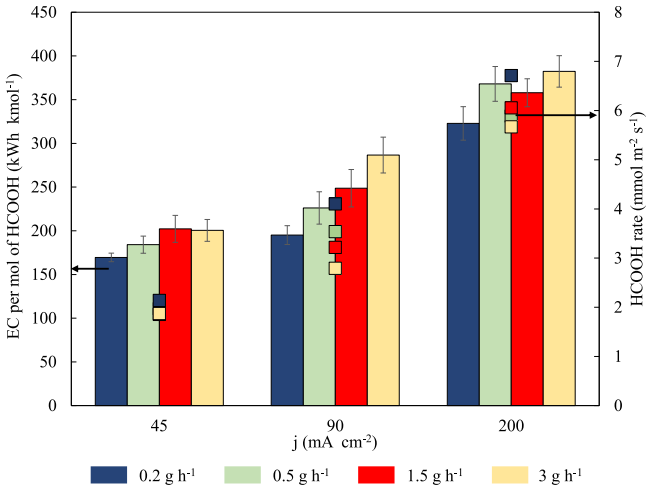

Fig. 8. Energy consumption and HCOOH rate in the three-compartment reactor as a function of j and water content in the feed CO_2 stream, with a fixed CO_2 feed flow rate of 20 ml min^{-1}.

current density of 90 mA cm^{-2} (Table S2). As presented in the Supporting Information, SPCE is primarily influenced by the CO_2 flow rate. However, other parameters, such as water content, also play a significant role. An increase in humidity in the CO_2 feed results in a lower SPCE, as it simultaneously reduces the FE toward formate formation.

At high *j* (200 mA cm^{-2}), bubble formation is observed in the central compartment's outlet stream. This is attributed to the decomposition of carbonate ions (CO_3^{2-}) transported from the cathodic compartment to the central compartment, where acidic conditions convert them into CO_2 [13].

The results of this study demonstrate that process performance strongly depends on *j*, water vapor content, and operational parameters. While higher *j* significantly enhances HCOOH production rates and concentrations (increasing by approximately 225 % when *j* is raised from 45 to 200 mA cm^{-2}), they also result in substantially higher energy consumption, with increases of up to 100 % observed over the same range. Additionally, increased water vapor content in the CO_2 feed stream adversely affects HCOOH concentration and FE, highlighting the need to balance production efficiency with energy consumption. These findings underscore the critical role of optimizing water vapor content and current density in the design and operation of three-compartment reactors for $ERCO_2$ to HCOOH.

3.2. *Two vs. three-compartment gas phase operation*

In this section, the performance of the three-reactor compartment presented in this work is compared with previously obtained results from two-compartment reactor similar experimental systems, enabling a rigorous comparison. The two-compartment reactor employs a Bi-GDE in a membrane electrode assembly (MEA) configuration with a Nafion 117 membrane, as described by Díaz-Sainz et al. [24]. In this setup, the cathodic compartment is fed with humidified CO_2, enabling direct comparison with the three-compartment electrolyzer evaluated in this study.

Fig. 9.a highlights the differences in $HCOOH/HCOO^-$ production between the two reactor configurations, evaluated in terms of production rate and FE. The three-compartment reactor demonstrates superior product formation rates at all *j*, with the difference becoming more pronounced as the j increases. At a *j* of 200 mA cm^{-2}, the three-compartment reactor achieves a formation rate of 5.88 mmol m^{-2} s^{-1}, 128 % higher than the 2.57 mmol m^{-2} s^{-1} achieved by the two-

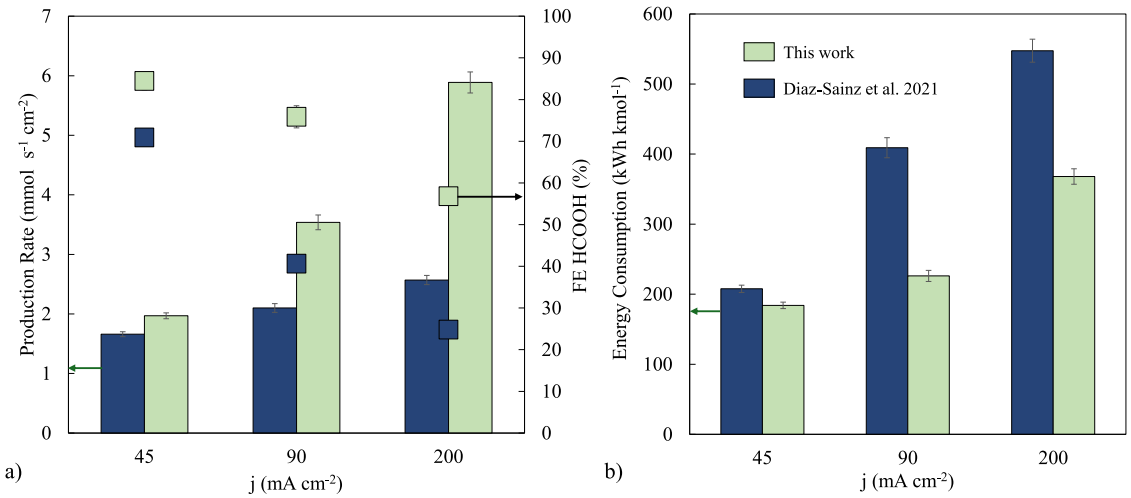

Fig. 9. a) Comparison of the results obtained for production rate and FE in this study with a two-compartment gas phase electrochemical cell [24], b) Comparison of the results obtained for EC this study with a two-compartment gas phase electrochemical cell [24].

compartment reactor.

Following this behaviour, the FE is consistently better for the three-compartment reactor, with the gap widening at higher *j*. In the case of 45 mA cm^{-2}, the three-compartment reactor achieves an FE of 84 %, compared to 71 % for the two-compartment reactor. When working at 90 mA cm^{-2}, the FE is 76 % for the three-compartment reactor and 41 % for the two-compartment reactor. The largest difference is observed at 200 mA cm^{-2}, where the three-compartment reactor achieves an FE of 57 %, more than double the 25 % obtained by the two-compartment reactor.

Fig. 9.b compares the performance in terms of EC. The three-compartment reactor exhibits a significant advantage due to its lower cell potentials and higher efficiency. For a 200 mA cm^{-2} *j*, it consumes 368 kWh $kmol^{-1}$, representing a 48 % reduction compared to the 709 kWh $kmol^{-1}$ recorded for the two-compartment reactor. Notably, the three-compartment reactor's EC at 200 mA cm^{-2} is lower than the two-compartment reactor's EC at 90 mA cm^{-2} (409 kWh $kmol^{-1}$). The energy efficiency of the three-compartment reactor is a critical advantage for industrial-scale implementation, as it leads to lower operational costs and a smaller carbon footprint. These benefits could be further enhanced by integrating renewable energy sources [8].

Another key difference lies in the nature of the product. The two-compartment reactor outputs $HCOO^-$, whereas the three-compartment reactor directly produces HCOOH, which is more valuable for industrial applications. The direct production of HCOOH eliminates the need for acidification, reducing reagent costs, minimizing the carbon footprint associated with acidolysis, and avoiding the generation of undesirable by products.

3.3. Performance analysis of the BPM electrolyzer

The BPM reactor is designed based on a two-compartment reactor, incorporating a BPM in reverse bias orientation, allowing for the dissociation of the water molecule into protons and hydroxide ions. To ensure BPM wetting and prevent the occurrence of high local overpotentials that could compromise the membrane stability, the reactor operates with a liquid catholyte. The reactor configuration and operating procedures are based on a setup previously used with a Nafion membrane [63]. The effect of varying catholyte ionic composition, concentration, and conductivity is evaluated to determine their impact on system performance. Detailed experimental results are presented in Tables S4 and S5 in the Supporting Information.

3.4. Use of different catholyte compositions

The performance of the BPM electrolyzer is assessed using different catholytes to maximize HCOOH production. Initially, 0.1 M KCl is employed as the catholyte, targeting the generation of an acidic product stream with a pH of approximately 3, indicating the direct production of HCOOH. This value is selected as the reference since the direct CO_2 electroreduction to formic acid occurs at pH values lower than the pKa of formic acid (3.77) [64].

Fig. 10a presents the concentration and FE of HCOOH at various flow rates (Qc/A) and current densities using 0.1 M KCl in the cathodic compartment. The highest concentration, 7.74 g L^{-1} is achieved at a Qc/A of 0.07 mL min^{-1} cm^{-2}, with an FE of 84 %, with a 45 mA cm^{-2} *j*. At the same *j*, lower concentrations of 0.92 g L^{-1} and 2.71 g L^{-1} are recorded at Qc/A values of 0.57 mL min^{-1} cm^{-2} and 0.15 mL min^{-1} cm^{-2}, respectively, with FEs of 82 % and 63 %. Increasing the *j* to 90 mA cm^{-2}, resulted in higher HCOOH concentrations, reaching 10.01 g L^{-1} at Qc/A of 0.07 mL min^{-1} cm^{-2}, while concentrations of 5.28 g L^{-1} and 1.95 g L^{-1} are observed at Qc/values of 0.15 and 0.57 mL min^{-1} cm^{-2}, respectively.

Fig. 10b illustrates the production rates and EC at different conditions using 0.1 M KCl in the cathodic compartment. At a *j* of 45 mA cm^{-2} and Qc/A of 0.07 mL min^{-1}, the highest formation rate, 1.96 mmol s^{-1} m^{-2}, is achieved, albeit with a high EC of 340 kWh $kmol^{-1}$. At 90 mA cm^{-2}, the maximum formation rate occurred at a Qc/A of 0.57 mL min^{-1} cm^{-2}, with an EC of 382 kWh $kmol^{-1}$.

As shown in Fig. 10, increasing the *j* consistently enhances HCOOH production. However, FE decreases slightly at higher *j*, except for the case of 0.07 mL min^{-1} cm^{-2}, where FE drops from 84 % at 45 mA cm^{-2} to 54 % at 90 mA cm^{-2}. The production rate increases with *j*, rising from 1.47 mmol s^{-1} m^{-2} to 2.87 mmol s^{-1} m^{-2} at a Qc/A of 0.15 mL min^{-1} cm^{-2}. However, energy consumption increases substantially, with a rise of nearly 180 % at a Qc/A of 0.07 mL min^{-1} cm^{-2}.

The Qc/A also significantly influences the process. Lower flow rates increase HCOOH concentration by up to 570 %, due to reduced product dilution. However, reduced flow rates result in lower FE, slower production rates, and increased cell voltages, likely due to thinning of the liquid film over the membrane, leading to a drier environment and higher EC. At 90 mA cm^{-2} and a Qc/A of 0.07 mL min^{-1} cm^{-2}, the EC reaches 610 kWh $kmol^{-1}$.

The BPM itself contributed to increased cell voltage, limiting operation to current densities below 100 mA cm^{-2}. To address these limitations, a more concentrated catholyte (0.5 M $KHCO_3$) is tested to reduce cell potential. Three flow rates are evaluated for each current density point: 0.57, 0.15, and 0.07 mL min^{-1} cm^{-2}.

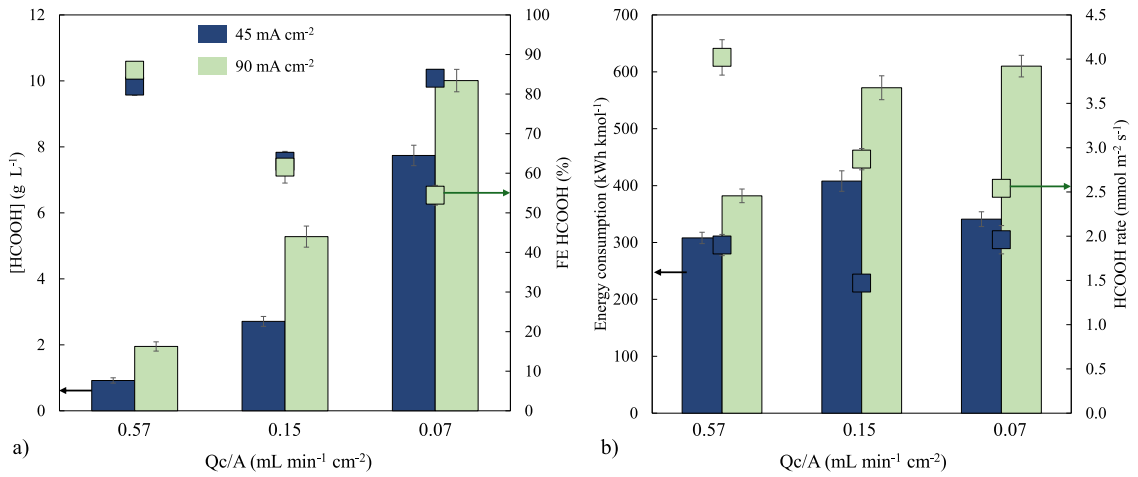

Fig. 10. a) HCOOH production in terms of concentration and FE, and b) HCOOH production rate and CE in the BPM electrolyzer membrane using 0.1 M KCl in the cathodic compartment as a function of current density and catholyte flow rate.

At a *j* of 45 mA cm^{-2} and a Qc/A of 0.57 mL min^{-1} cm^{-2}, a concentration of 1.02 g L^{-1} and an FE of 90 % are achieved. Higher concentrations of 3.94 g L^{-1} and 5.27 g L^{-1} are observed at Qc/A values of 0.15 mL min^{-1} cm^{-2} and 0.07 mL min^{-1} cm^{-2}, respectively, with corresponding FEs of 91 % and 58 % (Fig. 11a).

When working at 90 mA cm^{-2}, higher $HCOO^-$ concentrations are achieved: 1.89 g L^{-1} at Qc/A values of 0.57 and 7.9 g l^{-1} at 0.15 mL min^{-1} cm^{-2}. However, reducing the flow rate to 0.07 mL min^{-1} cm^{-2} slightly decreases the concentration to 7.81 g L^{-1} due to increased cell potential. On the other hand, for *j* of 200 mA cm^{-2}, production is feasible only with a Qc/A of 0.57 mL min^{-1} cm^{-2}, yielding a concentration of 3.03 g L^{-1} and an FE of 60 %. However, EC remained high, exceeding 764 kWh $kmol^{-1}$.

A comparison of 0.1 M KCl and 0.5 M $KHCO_3$ revealed similar performance at lower j. However, only 0.5 M $KHCO_3$ supported operation at 200 mA cm^{-2}. The effluent pH (6–7) from 0.5 M $KHCO_3$ produces $HCOO^-$ instead of HCOOH, reducing its economic appeal. Conversely, 0.1 M KCl directly produced HCOOH with a pH of ~3, making it the preferred electrolyte despite its limitations at current densities above 100 mA cm^{-2}. Furthermore, when evaluating the SPCE for both catholyte compositions (Tables S4 and S5), comparable values are obtained, ranging between 1 % and 2.5 %. Despite this similarity, the SPCE remains relatively low, primarily due to the operation with an excess CO_2 in the two-compartment reactor.

3.5. CEM vs. BPM liquid phase electrolyzer

This section analyzes and compares the performance of two reactor configurations in producing HCOOH and $HCOO^-$ during the $ERCO_2$ process. Fig. 12 compares the concentration of HCOOH/$HCOO^-$ and the EC in a two-compartment reactor using a BPM with 0.1 M KCl as the catholyte, against results from a previous study that employed 0.5 M KCl + 0.45 M $KHCO_3$ as the catholyte solution, employing a Nafion 117 as CEM [63].

Before discussing the results, it is important to highlight that while Díaz-Sainz et al. [63] focus on the production of $HCOO^-$, the present study achieves the direct production of HCOOH. Regarding process performance, Díaz-Sainz et al. [63] report higher efficiency. For a *j* of 90 mA cm^{-2} and a Qc/A of 0.57 mL min^{-1} cm^{-2}, Díaz-Sainz et al. achieve a concentration of 2.04 g L^{-1} with an EC of 177 kWh·$kmol^{-1}$. In contrast, this study achieves a similar concentration of 1.95 g L^{-1} but with a significantly higher EC of 364 kWh $kmol^{-1}$ when using 0.1 M KCl. This disparity in EC is attributed to Díaz-Sainz et al.'s reactor [63], due to the additional overpotential introduced by the BPM.

Under the same *j* (90 mA cm^{-2}) but with a reduced Qc/A of 0.15 mL min^{-1} cm^{-2}, Díaz-Sainz et al. report a concentration of 7.51 g L^{-1} and an EC of 186 kWh·$kmol^{-1}$. In comparison, the two-compartment BPM reactor in this study achieves a concentration of 5.28 g L^{-1} with an EC of 572 kWh·$kmol^{-1}$. These results demonstrate the superior performance of

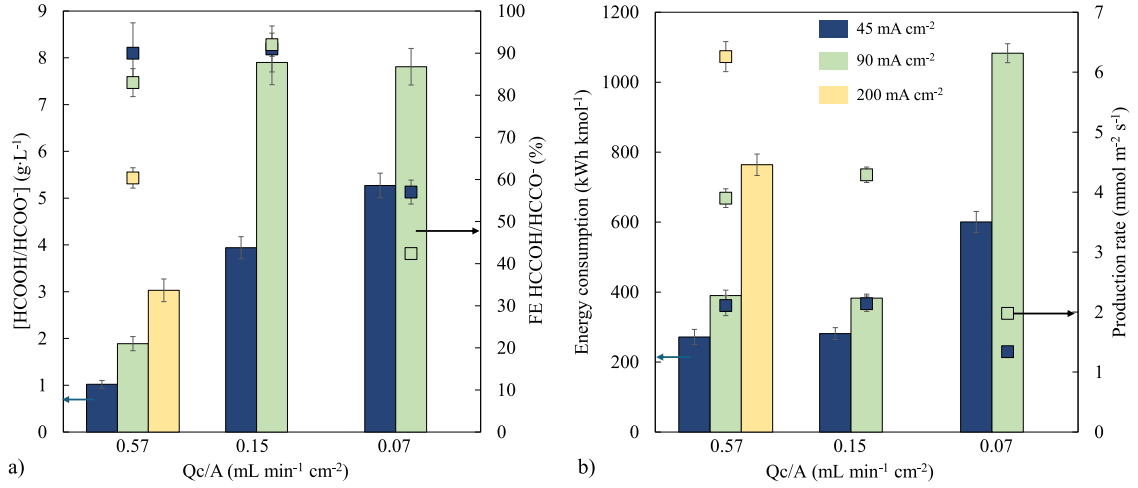

Fig. 11. a) Production in terms of concentration and FE, b) Production rate and energy consumption in the two-compartment reactor with a BPM using 0.5 M $KHCO_3$ in the cathodic compartment as a function of j and the catholyte flow rate.

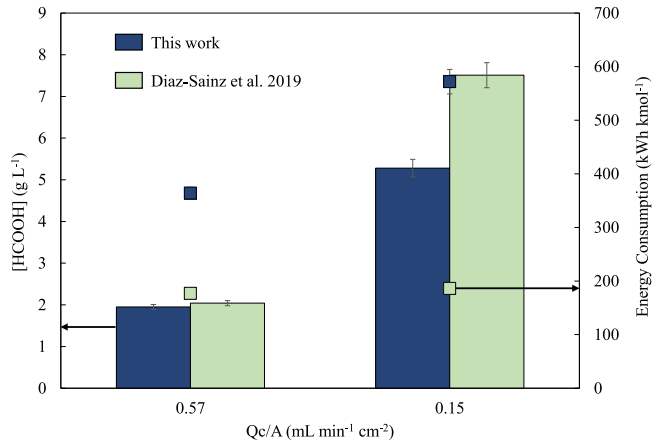

Fig. 12. Comparison of the results in terms of HCOOH/$HCOO^-$ concentration and EC in the two-compartment reactor with a bipolar membrane and 0.1 M KCl as liquid catholyte, compared to the study by Díaz-Sainz et al., [63].

Díaz-Sainz et al.'s process, both in terms of product concentration and energy efficiency.

Despite these differences, the BPM reactor offers a key advantage: it can directly produce HCOOH, a more valuable product than $HCOO^-$. Directly producing HCOOH eliminates the need for an acidolysis step, avoiding additional reagent costs, the carbon footprint of acidolysis reagents, and undesirable byproduct generation. While the BPM reactor currently exhibits higher energy consumption, its ability to produce HCOOH makes it a promising approach for industrial-scale applications.

In conclusion, the tests performed with the two-compartment reactor with a BPM represent a valuable starting point for the direct production of HCOOH. Further optimization is necessary to reduce energy consumption and improve overall process efficiency. However, the potential economic and environmental benefits of HCOOH production justify continued research in this direction.

When comparing the performance of the two CO_2 electrolyzer configurations, it is essential to consider not only the performance but also the reaction mechanism occurring in each system, as they exhibit differences. In the three-compartment reactor, the reaction environment remains neutral, leading to the electrochemical reduction of CO_2 to formate ions (Eq. (1)). These ions then combine with protons to form formic acid in the central compartment. Conversely, in the two-compartment reactor, the BPM facilitates the supply of protons to the cathodic compartment, creating an acidic reaction environment. In this case, rather than water molecules participating in the reaction, the protons generated from water dissociation act as the primary proton source. This results in the direct formation of formic acid at the cathode, as described in Eq. (2).

$$CO_2 + H_2O + 2e^- \rightarrow HCOO^- + OH^- \quad (1)$$

$$CO_2 + 2H^+ + 2e^- \rightarrow HCOOH \quad (2)$$

Each reactor configuration presents distinct challenges. In the case of the three-compartment reactor, the central compartment represents the most critical element for successful scaling. Given that this compartment consists of ion-exchange resins, ensuring their homogeneous distribution is essential to prevent localized flow blockages of deionized water or the formation of overpressures, both of which could compromise the overall reactor performance. Additionally, increasing the active electrode area may result in higher bubble generation within the central compartment due to byproduct formation (H_2 or CO). The accumulation of these gaseous species could lead to an increase in electrical resistance to ion transport, a key factor in maintaining low cell potentials.

In contrast, the two-compartment BPM reactor offers a potentially more straightforward scaling process due to its simpler configuration. However, its scaling challenges include achieving a uniform CO2 distribution across the gas diffusion electrode and maintaining the wettability of the BPM membrane to prevent degradation or functional impairments.

4. Conclusion

The primary objective of this study is successfully achieved, demonstrating the direct production of HCOOH with two novel reactor configurations. Among these, the three-compartment reactor yields the most promising results, positioning this technology as a strong candidate for industrial-scale implementation of $ERCO_2$. An in-depth analysis evaluates the effects of various operational parameters, including current density, CO_2 flow rate, and water content in the CO_2 feed, on process performance.

For the three-compartment reactor, optimal conditions are identified, revealing that HCOOH production increases with higher current densities and lower vapor flow rates. These findings highlight the importance of optimizing water content in the CO_2 feed and current density in the design and operation of three-compartment reactors for the electroreduction of CO_2 to HCOOH. In contrast, the CO_2 flow rate shows minimal influence on process efficiency. Operating at a current density of 200 mA cm^{-2}, with a CO_2 flow rate of 20 mL min^{-1} and a water content of 0.5 g h^{-1}, the reactor achieves an impressive HCOOH concentration of 125 g L^{-1} with an energy consumption of 368 kWh $kmol^{-1}$. These results underscore the reactor's potential for energy-efficient $ERCO_2$ at an industrial scale.

A two-compartment reactor with a bipolar membrane is then developed and tested under various electrolytes and operating conditions. The results show that 0.5 M $KHCO_3$ is unsuitable as it promotes formate formation due to its neutral pH. Conversely, a 0.1 M KCl solution proves effective for HCOOH production, except at high *j*, where elevated cell potentials reduce efficiency. Under optimal conditions, the reactor achieves an HCOOH concentration of 5.28 g L^{-1} with an energy consumption of 572 kWh $kmol^{-1}$, operating at 90 mA cm^{-2} with a Qc/A of 0.15 mL min^{-1} cm^{-2}.

To enhance the evaluated processes, several improvements are suggested for the two-compartment reactor with a bipolar membrane, including exploring alternative electrolytes to improve energy efficiency. Additionally, using advanced bipolar membranes further decreases cell potentials and energy consumption.

Both configurations demonstrate strong potential as viable pathways for the direct production of HCOOH via $ERCO_2$, showing similar or even improved performances as previously evaluated $ERCO_2$ top formate electrolyzers, with further optimization paving the way for their industrial application.

CRediT authorship contribution statement

Jose Antonio Abarca: Writing – original draft, Supervision, Methodology, Investigation, Formal analysis, Conceptualization. **Mario Coz-Cruz:** Methodology, Investigation, Data curation. **Manuel Alvarez-Guerra:** Writing – review & editing, Project administration, Funding acquisition, Formal analysis. **Guillermo Díaz-Sainz:** Conceptualization, Resources, Writing – review & editing, Supervision, Project administration, Funding acquisition. **Angel Irabien:** Writing – review & editing, Project administration, Funding acquisition, Formal analysis.

Declaration of competing interest

The authors declare that they have no known competing financial interests or personal relationships that could have appeared to influence the work reported in this paper.

Acknowledgments

The authors fully acknowledge the financial support received from the Spanish State Research Agency (AEI) through the projects PID2022–138491OB-C31 (MICIU/AEI /10.13039/501100011033 and ERDF/EU), and PLEC2022–009398 (MCIN/AEI/10.13039/501100011033 and Union Europea Next Generation EU/PRTR). The financial support from the "Complementary Plan in the area of Energy and Renewable Hydrogen" funded by the Autonomous Community of Cantabria, Spain, and the European Union Next Generation EU/PRTR, is also gratefully acknowledged. The present work is related to CAPTUS Project. This project has received funding from the European Union's Horizon Europe research and innovation programme under grant agreement No 101118265. The authors gratefully acknowledge the support of the Society for the Regional Development of Cantabria (SODERCAN Group) through Grants SB100513774 and SB100513775 (Convocatoria para el año 2023 de las subvenciones del programa de fomento de la economía circular) and Grant SB80988064 (Convocatoria para el año 2022 de las subvenciones correspondientes al programa de fomento de la transferencia tecnológica (INVESNOVA). Jose Antonio Abarca gratefully acknowledges the predoctoral research grant (FPI) PRE2021–097200.

Supplementary materials

Supplementary material associated with this article can be found, in the online version, at doi:10.1016/j.electacta.2025.146182.

Data availability

Data will be made available on request.

References

[1] Trends in CO2 - NOAA Global Monitoring Laboratory. https://gml.noaa.gov/ccgg/trends/. (accessed November 7, 2024).
[2] W. Zhang, Y. Hu, L. Ma, G. Zhu, Y. Wang, X. Xue, R. Chen, S. Yang, Z. Jin, rogress and Perspective of Electrocatalytic CO_2 Reduction for Renewable Carbonaceous Fuels and Chemicals, Adv. Sci. 5 (2018) 1700275, https://doi.org/10.1002/advs.201700275.
[3] P.R. Yaashikaa, P. Senthil Kumar, S.J. Varjani, A. Saravanan, A review on photochemical, biochemical and electrochemical transformation of CO_2 into value-added products, J. CO_2 Utili. 33 (2019) 131–147, https://doi.org/10.1016/J.JCOU.2019.05.017.
[4] S. Castro, J. Albo, A. Irabien, Photoelectrochemical Reactors for CO2 Utilization, ACS. Sustain. Chem. Eng. 6 (2018) 15877–15894, https://doi.org/10.1021/ACSSUSCHEMENG.8B03706.
[5] G. Díaz-Sainz, M. Alvarez-Guerra, J. Solla-Gullón, L. García-Cruz, V. Montiel, A. Irabien, Gas–liquid–solid reaction system for CO_2 electroreduction to formate without using supporting electrolyte, AIChe J. 66 (2020) e16299, https://doi.org/10.1002/AIC.16299.
[6] B.Endrődi Vass, C. Janáky, Coupling electrochemical carbon dioxide conversion with value-added anode processes: An emerging paradigm, Curr. Opin. Electrochem. 25 (2021) 100621, https://doi.org/10.1016/J.COELEC.2020.08.003.
[7] D. Du, R. Lan, J. Humphreys, S. Tao, Progress in inorganic cathode catalysts for electrochemical conversion of carbon dioxide into formate or formic acid, J. Appl. Electrochem. 47 (2017) 661–678, https://doi.org/10.1007/S10800-017-1078-X.
[8] M. Rumayor, A. Dominguez-Ramos, P. Perez, A. Irabien, A techno-economic evaluation approach to the electrochemical reduction of CO_2 for formic acid manufacture, J. CO_2 Utili. 34 (2019) 490–499, https://doi.org/10.1016/J.JCOU.2019.07.024.
[9] Formic Acid Market Size, Share, Trends, Growth & Forecast. https://www.chemanalyst.com/industry-report/formic-acid-market-688 (accessed November 7, 2024).
[10] X. Zhang, M. Jiao, Z. Chen, X. Ma, Z. Wang, N. Wang, X. Zhang, L. Liu, An integrated gradually thinning and dual-ion co-substitution strategy modulated In-O-ultrathin-SnS_2 nanosheets to achieve efficient electrochemical reduction of CO_2, Chem. Eng. J. 429 (2022) 132145, https://doi.org/10.1016/J.CEJ.2021.132145.
[11] Y. Shi, Y. Ji, J. Long, Y. Liang, Y. Liu, Y. Yu, J. Xiao, B. Zhang, Unveiling hydrocerussite as an electrochemically stable active phase for efficient carbon dioxide electroreduction to formate, Nat. Commun. 11 (2020) 3415, https://doi.org/10.1038/s41467-020-17120-9.
[12] A. Löwe, C. Rieg, T. Hierlemann, N. Salas, D. Kopljar, N. Wagner, E. Klemm, Influence of Temperature on the Performance of Gas Diffusion Electrodes in the CO_2 Reduction Reaction, ChemElectroChem. 6 (2019) 4497–4506, https://doi.org/10.1002/celc.201900872.
[13] H. Yang, J.J. Kaczur, S.D. Sajjad, R.I. Masel, Electrochemical conversion of CO_2 to formic acid utilizing Sustainion™ membranes, J. CO_2 Utili 20 (2017) 208–217, https://doi.org/10.1016/j.jcou.2017.04.011.
[14] K. Fernández-Caso, G. Díaz-Sainz, M. Alvarez-Guerra, A. Irabien, Electroreduction of CO_2: Advances in the Continuous Production of Formic Acid and Formate, ACS. Energy Lett. 8 (2023) 1992–2024, https://doi.org/10.1021/ACSENERGYLETT.3C00489.
[15] J. Lee, H. Liu, Y. Chen, W. Li, Bismuth Nanosheets Derived by in Situ Morphology Transformation of Bismuth Oxides for Selective Electrochemical CO_2 Reduction to Formate, ACS. Appl. Mater. Interfaces. 14 (2022) 14210–14217, https://doi.org/10.1021/ACSAMI.1C25217.
[16] S. Liu, C. Wang, J. Wu, B. Tian, Y. Sun, Y. Lv, Z. Mu, Y. Sun, X. Li, F. Wang, Y. Wang, L. Tang, P. Wang, Y. Li, M. Ding, Efficient CO_2 Electroreduction with a Monolayer Bi_2WO_6 through a Metallic Intermediate Surface State, ACS. Catal. 11 (2021) 12476–12484, https://doi.org/10.1021/ACSCATAL.1C02495.
[17] L. Li, A. Ozden, S. Guo, F.P. García de Arquer, C. Wang, M. Zhang, J. Zhang, H. Jiang, W. Wang, H. Dong, D. Sinton, E.H. Sargent, M. Zhong, Stable, active CO_2 reduction to formate via redox-modulated stabilization of active sites, Nat. Commun. 12 (2021) 5223, https://doi.org/10.1038/s41467-021-25573-9.
[18] Y. Xing, X. Kong, X. Guo, Y. Liu, Q. Li, Y. Zhang, Y. Sheng, X. Yang, Z. Geng, J. Zeng, Bi@Sn Core–Shell Structure with Compressive Strain Boosts the Electroreduction of CO_2 into Formic Acid, Adv. Sci. 7 (2020) 1902989, https://doi.org/10.1002/ADVS.201902989.
[19] P.F. Sui, C. Xu, M.N. Zhu, S. Liu, Q. Liu, J.L. Luo, Interface-Induced Electrocatalytic Enhancement of CO_2-to-Formate Conversion on Heterostructured Bismuth-Based Catalysts, Small. 18 (2022) 2105682, https://doi.org/10.1002/SMLL.202105682.
[20] Z. Wang, Y. Zhou, D. Liu, R. Qi, C. Xia, M. Li, B. You, B.Y. Xia, Carbon-Confined Indium Oxides for Efficient Carbon Dioxide Reduction in a Solid-State Electrolyte Flow Cell, Angew. Chem. Int. Ed. 61 (2022) e202200552, https://doi.org/10.1002/ANIE.202200552.
[21] T. Zheng, C. Liu, C. Guo, M. Zhang, X. Li, Q. Jiang, W. Xue, H. Li, A. Li, C.W. Pao, J. Xiao, C. Xia, J. Zeng, Copper-catalysed exclusive CO_2 to pure formic acid conversion via single-atom alloying, Nat. Nanotechnol. 16 (2021) 1386–1393, https://doi.org/10.1038/s41565-021-00974-5.
[22] L. Fan, C. Xia, P. Zhu, Y. Lu, H. Wang, Electrochemical CO_2 reduction to high-concentration pure formic acid solutions in an all-solid-state reactor, Nat. Commun. 11 (2020) 3633, https://doi.org/10.1038/s41467-020-17403-1.
[23] C. Xia, P. Zhu, Q. Jiang, Y. Pan, W. Liang, E. Stavitsk, H.N. Alshareef, H. Wang, Continuous production of pure liquid fuel solutions via electrocatalytic CO_2 reduction using solid-electrolyte devices, Nat. Energy 4 (2019) 776–785, https://doi.org/10.1038/s41560-019-0451-x.
[24] G. Díaz-Sainz, M. Alvarez-Guerra, B. Ávila-Bolívar, J. Solla-Gullón, V. Montiel, A. Irabien, Improving trade-offs in the figures of merit of gas-phase single-pass continuous CO_2 electrocatalytic reduction to formate, Chem. Eng. J. 405 (2021) 126965, https://doi.org/10.1016/J.CEJ.2020.126965.
[25] Y. Wu, H. Rabiee, X.S. Zhao, G. Wang, Y. Jiang, Insights into electrolyte flooding in flexible gas diffusion electrodes for CO_2 electrolysis: from mechanisms to effective mitigation strategies, J. Mater. Chem. a Mater. 12 (2024) 14206–14228, https://doi.org/10.1039/d4ta01994f.
[26] J. Disch, L. Bohn, L. Metzler, S. Vierrath, Strategies for the mitigation of salt precipitation in zero-gap CO_2 electrolyzers producing CO, J. Mater. Chem. a Mater. 11 (2023) 7344–7357, https://doi.org/10.1039/D2TA09966G.
[27] B. Rutjens, K. von Foerster, B. Schmid, H. Weinrich, S. Sanz, H. Tempel, R. A. Eichel, Impact of the PiperION Anion Exchange Membrane Thickness on the Performance of a CO_2-to-HCOOH Three-Compartment Electrolyzer, Ind. Eng. Chem. Res. 63 (2024) 3986–3996, https://doi.org/10.1021/acs.iecr.3c04459.
[28] H. Yang, J.J. Kaczur, S.D. Sajjad, R.I. Masel, Performance and long-term stability of CO_2 conversion to formic acid using a three-compartment electrolyzer design, J. CO_2 Utili 42 (2020) 101349, https://doi.org/10.1016/J.JCOU.2020.101349.
[29] B. Endrődi, G. Bencsik, F. Darvas, R. Jones, K. Rajeshwar, C. Janáky, Continuous-flow electroreduction of carbon dioxide, Prog. Energy Combust. Sci. 62 (2017) 133–154, https://doi.org/10.1016/j.pecs.2017.05.005.
[30] Z. Xing, X. Hu, X. Feng, Tuning the Microenvironment in Gas-Diffusion Electrodes Enables High-Rate CO_2 Electrolysis to Formate, ACS. Energy Lett. 6 (2021) 1694–1702, https://doi.org/10.1021/ACSENERGYLETT.1C00612.
[31] M. Fan, S. Prabhudev, S. Garbarino, J. Qiao, G.A. Botton, D.A. Harrington, A. C. Tavares, D. Guay, Uncovering the nature of electroactive sites in nano architectured dendritic Bi for highly efficient CO_2 electroreduction to formate, Appl. Catal. B 274 (2020) 119031, https://doi.org/10.1016/J.APCATB.2020.119031.
[32] B. De Mot, J. Hereijgers, M. Duarte, T. Breugelmans, Influence of flow and pressure distribution inside a gas diffusion electrode on the performance of a flow-by CO_2 electrolyzer, Chem. Eng. J. 378 (2019) 122224, https://doi.org/10.1016/J.CEJ.2019.122224.
[33] I. Merino-Garcia, J. Albo, A. Irabien, Tailoring gas-phase CO_2 electroreduction selectivity to hydrocarbons at Cu nanoparticles, Nanotechnology. 29 (2018) 014001, https://doi.org/10.1088/1361-6528/aa994e.
[34] H. Li, C. Oloman, Development of a continuous reactor for the electro-reduction of carbon dioxide to formate - Part 2: Scale-up, J. Appl. Electrochem. 37 (2007) 1107–1117, https://doi.org/10.1007/S10800-007-9371-8.
[35] Z. Liu, X. Lv, J. Zhang, A. Guan, C. Yang, S. Yan, Y. Chen, K. Liu, G. Zheng, Hydroxy-Group-Enriched In_2O_3 Facilitates CO_2 Electroreduction to Formate at Large Current Densities, Adv. Mater. Interfaces. 9 (2022) 2101956, https://doi.org/10.1002/ADMI.202101956.
[36] H.R. Jhong, U.O. Nwabara, S. Shubert-Zuleta, N.S. Grundish, B. Tandon, L. C. Reimnitz, C.M. Staller, G.K. Ong, C.A. Saez Cabezas, J.B. Goodenough, P.J.

A. Kenis, D.J. Milliron, Efficient Aqueous Electroreduction of CO_2 to Formate at Low Overpotential on Indium Tin Oxide Nanocrystals, Chem. Mater. 33 (2021) 7675–7685, https://doi.org/10.1021/ACS.CHEMMATER.1C01649.
[37] Q. Gong, P. Ding, M. Xu, X. Zhu, M. Wang, J. Deng, Q. Ma, N. Han, Y. Zhu, J. Lu, Z. Feng, Y. Li, W. Zhou, Y. Li, Structural defects on converted bismuth oxide nanotubes enable highly active electrocatalysis of carbon dioxide reduction, Nat. Commun. 10 (2019) 2807, https://doi.org/10.1038/s41467-019-10819-4.
[38] J. Wang, J. Zou, X. Hu, S. Ning, X. Wang, X. Kang, S. Chen, Heterostructured intermetallic CuSn catalysts: high performance towards the electrochemical reduction of CO_2 to formate, J. Mater. Chem. a Mater. 7 (2019) 27514–27521, https://doi.org/10.1039/C9TA11140A.
[39] K. Yao, H. Wang, X. Yang, Y. Huang, C. Kou, T. Jing, S. Chen, Z. Wang, Y. Liu, H. Liang, Metal-organic framework derived dual-metal sites for electroreduction of carbon dioxide to HCOOH, Appl. Catal. B 311 (2022) 121377, https://doi.org/10.1016/J.APCATB.2022.121377.
[40] I.Zelocualtecatl Montiel, A. Dutta, K. Kiran, A. Rieder, A. Iarchuk, S. Vesztergom, M. Mirolo, I. Martens, J. Drnec, P. Broekmann, CO_2 Conversion at High Current Densities: Stabilization of Bi(III)-Containing Electrocatalysts under CO_2 Gas Flow Conditions, ACS. Catal. 12 (2022) 10872–10886, https://doi.org/10.1021/ACSCATAL.2C02549.
[41] J. Yang, X. Wang, Y. Qu, X. Wang, H. Huo, Q. Fan, J. Wang, L.M. Yang, Y. Wu, Bi-Based Metal-Organic Framework Derived Leafy Bismuth Nanosheets for Carbon Dioxide Electroreduction, Adv. Energy Mater. 10 (2020) 2001709, https://doi.org/10.1002/AENM.202001709.
[42] G. Díaz-Sainz, M. Alvarez-Guerra, A. Irabien, Continuous electroreduction of CO_2 towards formate in gas-phase operation at high current densities with an anion exchange membrane, J. CO_2 Utili. 56 (2022) 101822, https://doi.org/10.1016/J.JCOU.2021.101822.
[43] Y.X. Duan, Y.T. Zhou, Z. Yu, D.X. Liu, Z. Wen, J.M. Yan, Q. Jiang, Boosting Production of HCOOH from CO_2 Electroreduction via Bi/CeO_x, Angew. Chem. Int. Ed. 60 (2021) 8798–8802, https://doi.org/10.1002/anie.202015713.
[44] Efficient CO_2 Reduction to HCOOH with High Selectivity and Energy Efficiency over Bi/rGO Catalyst, Small. Methods 4 (2020) 1900846, https://doi.org/10.1002/SMTD.201900846.
[45] Y. Xing, H. Chen, Y. Liu, Y. Sheng, J. Zeng, Z. Geng, J. Bao, A phosphate-derived bismuth catalyst with abundant grain boundaries for efficient reduction of CO_2 to HCOOH, Chem. Commun. 57 (2021) 1502–1505, https://doi.org/10.1039/D0CC06756C.
[46] F.L. Meng, Q. Zhang, K.H. Liu, X.B. Zhang, Integrated Bismuth Oxide Ultrathin Nanosheets/Carbon Foam Electrode for Highly Selective and Energy-Efficient Electrocatalytic Conversion of CO_2 to HCOOH, Chem. Eur. J. 26 (2020) 4013–4018, https://doi.org/10.1002/chem.201903158.
[47] C. Wang, R. Pang, Z. Pan, Y. Zhu, C. Li, B. Liu, J. Shen, The interfacial aspect of Bi_2O_3/CeOx heterostructure catalysts for HCOOH production from CO_2 electroreduction, J. Mater. Chem. a Mater. 10 (2022) 22694–22700, https://doi.org/10.1039/d2ta06640h.
[48] J.W. Shi, S.N. Sun, J. Liu, Q. Niu, L.Z. Dong, Q. Huang, J.J. Liu, R. Wang, Z. Xin, D. Zhang, J. Niu, Y.Q. Lan, Calixarene-Functionalized Stable Bismuth Oxygen Clusters for Specific CO_2-to-HCOOH Electroreduction, ACS. Catal. 12 (2022) 14436–14444, https://doi.org/10.1021/acscatal.2c02715.
[49] X.Du Liang, N. Tian, S.N. Hu, Z.Y. Zhou, S.G. Sun, Recent advances of bismuth-based electrocatalysts for CO_2 reduction: Strategies, mechanism and applications, Mater. Rep. Energy 3 (2023) 100191, https://doi.org/10.1016/J.MATRE.2023.100191.
[50] B. Sun, Z. Li, D. Xiao, H. Liu, K. Song, Z. Wang, Y. Liu, Z. Zheng, P. Wang, Y. Dai, B. Huang, A. Thomas, H. Cheng, Unveiling pH-Dependent Adsorption Strength of $*CO_2^-$ Intermediate over High-Density Sn Single Atom Catalyst for Acidic CO_2-to-HCOOH Electroreduction, Angew. Chem. Int. Ed. 63 (2024) e202318874, https://doi.org/10.1002/anie.202318874.
[51] Y. Wang, C. Wang, Y. Wei, F. Wei, L. Kong, J. Feng, J.Q. Lu, X. Zhou, F. Yang, Efficient and Selective Electroreduction of CO_2 to HCOOH over Bismuth-Based Bromide Perovskites in Acidic Electrolytes, Chem. Eur. J. 28 (2022) e202201832, https://doi.org/10.1002/chem.202201832.
[52] K. Xie, R.K. Miao, A. Ozden, S. Liu, Z. Chen, C.T. Dinh, J.E. Huang, Q. Xu, C. M. Gabardo, G. Lee, J.P. Edwards, C.P. O'Brien, S.W. Boettcher, D. Sinton, E. H. Sargent, Bipolar membrane electrolyzers enable high single-pass CO_2 electroreduction to multicarbon products, Nat. Commun. 13 (2022) 3609, https://doi.org/10.1038/s41467-022-31295-3.
[53] M.A. Blommaert, R. Sharifian, N.U. Shah, N.T. Nesbitt, W.A. Smith, D.A. Vermaas, Orientation of a bipolar membrane determines the dominant ion and carbonic species transport in membrane electrode assemblies for CO_2 reduction, J. Mater. Chem. a Mater. 9 (2021) 11179–11186, https://doi.org/10.1039/D0TA12398F.
[54] Y. Kang, T. Kim, K.Y. Jung, K.T. Park, Recent Progress in Electrocatalytic CO_2 Reduction to Pure Formic Acid Using a Solid-State Electrolyte Device, Catalysts. 13 (2023) 955, https://doi.org/10.3390/catal13060955.
[55] J.A. Abarca, G. Díaz-Sainz, A. Irabien, Inhibiting salt precipitation on the gas diffusion electrode surface in gas-phase CO_2 electroreduction to formate by using an acidic anolyte, J. CO_2 Utili. 86 (2024) 102897, https://doi.org/10.1016/J.JCOU.2024.102897.
[56] W. Zhang, Y. Hu, L. Ma, G. Zhu, Y. Wang, X. Xue, R. Chen, S. Yang, Z. Jin, Progress and Perspective of Electrocatalytic CO_2 Reduction for Renewable Carbonaceous Fuels and Chemicals, Adv. Sci. 5 (2018) 1700275, https://doi.org/10.1002/ADVS.201700275.
[57] Y.Y. Birdja, E. Pérez-Gallent, M.C. Figueiredo, A.J. Göttle, F. Calle-Vallejo, M.T. M. Koper, Advances and challenges in understanding the electrocatalytic conversion of carbon dioxide to fuels, Nat. Energy 4 (2019) 732–745, https://doi.org/10.1038/s41560-019-0450-y.
[58] J.W. Blake, J.T. Padding, J.W. Haverkort, Analytical modelling of CO_2 reduction in gas-diffusion electrode catalyst layers, Electrochim. Acta 393 (2021) 138987, https://doi.org/10.1016/j.electacta.2021.138987.
[59] F. Bienen, D. Kopljar, A. Löwe, S. Geiger, N. Wagner, E. Klemm, K.A. Friedrich, Revealing Mechanistic Processes in Gas-Diffusion Electrodes during CO_2 Reduction via Impedance Spectroscopy, ACS. Sustain. Chem. Eng. 8 (2020) 13759–13768, https://doi.org/10.1021/acssuschemeng.0c04451.
[60] M. Moura de Salles Pupo, R. Kortlever, Electrolyte Effects on the Electrochemical Reduction of CO_2, Chemphyschem. 20 (2019) 2926–2935, https://doi.org/10.1002/CPHC.201900680.
[61] Y.J. Sa, C.W. Lee, S.Y. Lee, J. Na, U. Lee, Y.J. Hwang, Catalyst–electrolyte interface chemistry for electrochemical CO_2 reduction, Chem. Soc. Rev. 49 (2020) 6632–6665, https://doi.org/10.1039/D0CS00030B.
[62] G. Díaz-Sainz, J.A. Abarca, M. Alvarez-Guerra, A. Irabien, Exploring the impact of partial pressure and typical compounds on the continuous electroconversion of CO_2 into formate, J. CO_2 Utili. 81 (2024) 102735, https://doi.org/10.1016/j.jcou.2024.102735.
[63] G. Díaz-Sainz, M. Alvarez-Guerra, J. Solla-Gullón, L. García-Cruz, V. Montiel, A. Irabien, CO_2 electroreduction to formate: Continuous single-pass operation in a filter-press reactor at high current densities using Bi gas diffusion electrodes, J. CO_2 Utili. 34 (2019) 12–19, https://doi.org/10.1016/j.jcou.2019.05.035.
[64] M. Oßkopp, A. Löwe, C.M.S. Lobo, S. Baranyai, T. Khoza, M. Auinger, E. Klemm, Producing formic acid at low pH values by electrochemical CO_2 reduction, J. CO_2 Utili. 56 (2022) 101823, https://doi.org/10.1016/J.JCOU.2021.101823.